

Tau-PET abnormality as a biomarker for Alzheimer's disease staging and early detection: a topological perspective

Jie Ding¹, Chushu Shen¹, Zhenguo Wang¹, Yongfeng Yang¹, Georges El Fakhri², Jie Lu³, Dong Liang¹, Hairong Zheng¹, Yun Zhou^{4,5}, Tao Sun^{1,6,*}, For the Alzheimer's Disease Neuroimaging Initiative and the Harvard Brain Aging Study

¹Paul C. Lauterbur Research Center for Biomedical Imaging, Shenzhen Institute of Advanced Technology, Chinese Academy of Sciences, Shenzhen 100864, People's Republic of China,

²Gordon Center for Medical Imaging, Department of Radiology, Massachusetts General Hospital, Harvard Medical School, Boston, Massachusetts 02114, United States,

³Department of Radiology and Nuclear Medicine, Xuanwu Hospital, Capital Medical University, Beijing 100053, People's Republic of China,

⁴Central Research Institute, United Imaging Healthcare Group Co., Ltd, Shanghai 201807, People's Republic of China,

⁵School of Biomedical Engineering, Shanghai Tech University, Shanghai 201210, People's Republic of China,

⁶United Imaging Research Institute of Innovative Medical Equipment, Shenzhen 518055, People's Republic of China

*Corresponding author: Xueyuan Avenue 1068, Nanshan District, Shenzhen, Guangdong, China. Email: tao.sun@siat.ac.cn

Alzheimer's disease can be detected early through biomarkers such as tau positron emission tomography (PET) imaging, which shows abnormal protein accumulations in the brain. The standardized uptake value ratio (SUVR) is often used to quantify tau-PET imaging, but topological information from multiple brain regions is also linked to tau pathology. Here a new method was developed to investigate the correlations between brain regions using subject-level tau networks. Participants with cognitive normal (74), early mild cognitive impairment (35), late mild cognitive impairment (32), and Alzheimer's disease (40) were included. The abnormality network from each scan was constructed to extract topological features, and 7 functional clusters were further analyzed for connectivity strengths. Results showed that the proposed method performed better than conventional SUVR measures for disease staging and prodromal sign detection. For example, when to differ healthy subjects with and without amyloid deposition, topological biomarker is significant with $P < 0.01$, SUVR is not with $P > 0.05$. Functionally significant clusters, i.e. medial temporal lobe, default mode network, and visual-related regions, were identified as critical hubs vulnerable to early disease conversion before mild cognitive impairment. These findings were replicated in an independent data cohort, demonstrating the potential to monitor the early sign and progression of Alzheimer's disease from a topological perspective for individual.

Key words: Alzheimer's disease; Tau-PET; Topological analysis; Staging; Early diagnosis.

Introduction

Neurofibrillary tangles (NFT) are caused by hyperphosphorylated tau buildup in the brain. Alzheimer's disease patients have NFT even during the normal cognitive stage (Cho et al. 2016). Transentorhinal areas of the medial temporal lobe often show early tau accumulation (Johnson et al. 2016). As the illness progressed, this accumulation gradually spread to the cerebral cortex (Braak and Braak 1995).

Positron emission tomography (PET) is a noninvasive imaging technology that can detect tau accumulation. Radioactive tracer such as ¹⁸F-flortaucipir (18F-AV-1451) is injected into the vein and binds to specific types of NFT in the brain (Chien et al. 2013; Xia et al. 2013). The difference in tracer uptake between gray matter and surrounding white matter can be visually examined. Although visual evaluation agrees well with postmortem results (Leuzy et al. 2019), it relies on expertise from nuclear medicine physicians (Tian et al. 2022). Another method to quantify a tau-PET scan is the standardized uptake value ratio (SUVR), which compares the target area's mean uptake value with that of the reference region's. Unlike the diffuse amyloid- β distribution, which

is assessed as global cortical uptake, tau accumulation has a hierarchical spread pattern (Schöll et al. 2016). "AD-signature" areas with higher tau accumulation rates were used to differentiate Alzheimer's disease stages (Jack et al. 2017; Maass et al. 2017), and found to correlate with cerebral cortical atrophy (Xia et al. 2017; Pelkmans et al. 2021) and also inverse correlate with glucose metabolism (Ossenkoppele et al. 2016; Whitwell et al. 2018). Several investigations have duplicated in vivo Braak staging using 18F-Flortaucipir scans (Schöll et al. 2016; Schwarz et al. 2016; Biel et al. 2021). While SUVR is complimentary to visual evaluation, it may not capture individual-specific tracer uptake pattern (Ossenkoppele et al. 2016; Young et al. 2022), just like Braak staging may not apply to individuals with abnormal tau accumulation in the neocortex and cortices (Ferreira et al. 2020).

Recently, topological analysis has been acknowledged as a powerful research tool for neurodegenerative diseases (Rubinov and Sporns 2010; Seghier and Price 2018; de Schotten and Forkel 2022). Such an approach aims to analyze data with underlying geometric structures from high-dimensional relationships, which can be effective for analyzing the image from a global

perspective rather than a regional one. Most of the existing efforts were based on magnetic resonance imaging (MRI) imaging; for example, diffusion tensor imaging offers structural information on axonal pathways, while functional MRI provides correlations of the blood-oxygenation-level-dependent signal between brain regions (Iturria-Medina et al. 2007; Zalesky and Fornito 2009; Galvin et al. 2011). Structural and functional connectivity can be measured either at group or individual level. On the other hand, metabolic connectivity using ^{18}F -FDG-PET is mostly based on group level analysis (Yakushev et al. 2017; Sala and Perani 2019). Several studies attempt to distinguish disease stages by comparing metabolic connectivity in-between groups (Chung et al. 2016; Huang et al. 2018; Li and Chen 2019). The accumulation of the NFT, on the other hand, is not evenly distributed but rather follows a predictable spatial pattern in the brain. For example, the group-level connectivity pattern was found following the intrinsic network or the gradient of the genes by studying the cross-sectional participants (Ossenkuppele et al. 2019; Montal et al. 2022). The derived connectivity often only reflects the average group connection but may not resolve the tau deposition heterogeneity in individual. Some recent studies have suggested deriving the FDG metabolic connectivity at the individual brain level based on relationships in regional activities (Huang et al. 2020; Wang et al. 2020; Yakushev et al. 2022).

In light of these previous efforts, we hypothesize that tau-PET topological measures could serve as staging markers and correlate with clinical outcome. Inter- and intra- correlations of clusters that containing regions with similar functions were of interest. The proposed framework aims to derive the biomarkers to (1) perform more accurate staging than conventional composite SUVR, (2) identify functional hubs sensitive to early disease conversion before mild cognitive impairment (MCI), and (3) associate disease progression at the individual level. We examined across different subject groups and compared the derived topological biomarkers with clinical outcome. The primary findings were replicated in 2 independent cohorts.

Materials and methods

Datasets and demographics

The Alzheimer's Disease Neuroimaging Initiative (ADNI) (Petersen et al. 2010) provided the data in this study. The included subjects were classified into 4 groups: normal cognition (CN, 74), early mild cognitive impairment (EMCI, 35), late mild cognitive impairment (LMCI, 32), and Alzheimer's disease (40), based on a combination of clinical symptoms and neurophysiological tests. EMCI or LMCI was confirmed based on the WMS-R Logical Memory II Story A score (Edmonds et al. 2019). The CN group was further subdivided into amyloid-negative (CN-, 48) and amyloid-positive (CN+, 26). The CN- group acted as the healthy control, while the other 4 acted as the patient groups. Before each scan, the patient underwent cognitive assessment, including the Mini-Mental State Examination (MMSE) and the Clinical Dementia Rating (CDR). The Harvard Brain Aging Study (HABS) (Dagley et al. 2017) was used as an independent data cohort to validate the conclusion. The included dataset consisted of 34 CN-, 21 CN+, and 11 with MCI. Table 1 shows the demographic information of 2 data cohorts.

Image acquisition and processing

In ADNI, all individuals underwent T1-weighted MRI and ^{18}F -flortaucipir PET scans. Tau-PET images were acquired 75 min after radiotracer injection and lasted 30 min (6 frames). For each individual, MRI scan was picked with the closest date to the PET

scan (mean interval time of 2 months, no more than 6 months). All subsequent processing was performed in Matlab R2018b unless otherwise stated. Smoothed reconstructed images were used to attain a spatial resolution of 8 mm. Motion correction was applied to dynamic images with a frame-by-frame registration process. Geometric Transfer Matrix method was used for partial volume correction (Rousset et al. 1998) before quantifying the regions of interests (ROIs). Brain parcellation was accomplished by registering PET images to their corresponding MR volume, which was previously segmented using Freesurfer 7.1.1 (<http://surfer.nmr.mgh.harvard.edu>). Consequently, the mean SUVR at each ROI was calculated by dividing the mean uptake of that region by the mean uptake of the whole cerebellum. The mean SUVR of all ROIs can then be utilized to build individual tau-PET network. For comparison, composite SUVR was calculated by averaging SUVRs from the Braak staging regions (Maass et al. 2017).

As stated earlier, the CN group was divided into 2 sub-groups: one with positive amyloid- β deposition (CN+) and one without evident deposition (CN-). This was confirmed by Amyloid-PET scan that was performed 50 min after the injection of ^{18}F -flaubetapir for a total of 20 min (4 frames). Patients having $\text{SUVR} > 1.11$ at distinctive ROIs were considered amyloid-positive (Landau et al. 2012).

Network construction and feature extraction

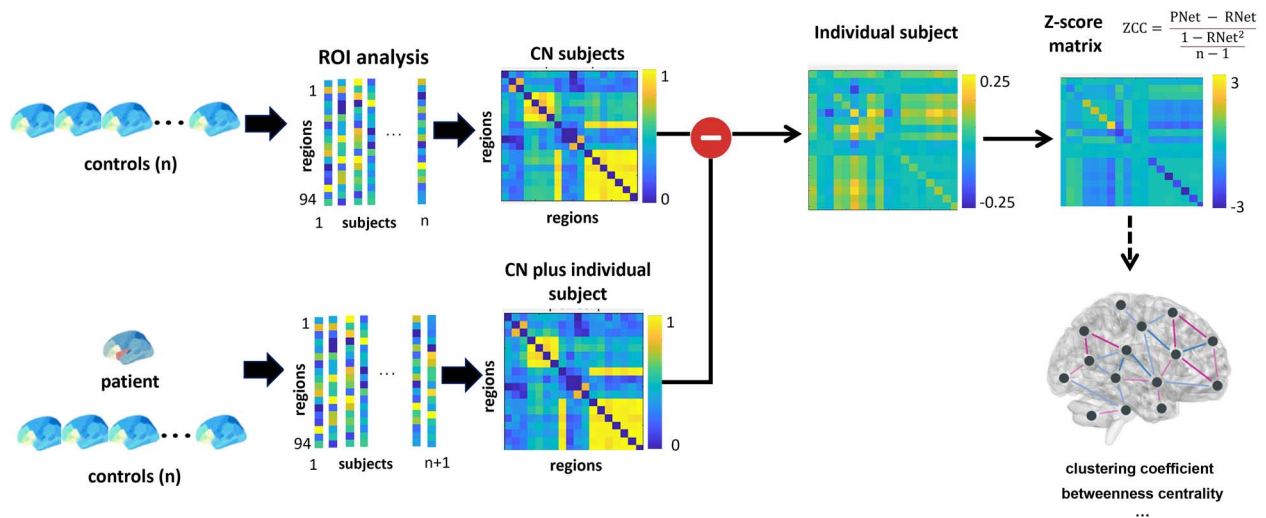
As stated in Introduction, the structure of the brain imaging data can be analyzed using the graph theory, thus allowing us to assess topological features qualitatively and quantitatively. Graph-based connectivity measurements can characterize the underlying network topology, where the similarity of regional property across subjects is measured as connectivity. For PET, the most obvious regional property is SUVR, for which the correlation analysis such as partial Pearson coefficients can be computed between regions (Sala et al. 2023). The resulting weighted, undirected network matrix has nodes representing regions and edges representing the strength of the connections. By quantifying the changes in the connectivity, it becomes possible to determine the status of various neurological diseases at group level.

Conventional group-level network only reflects the average topological information within the group, while disregarding the individual difference. We adapted a recently developed method to detect metabolic abnormalities, which creates individual network connectivity based on a whole-body FDG-PET scan (Sun et al. 2022). The following steps are executed to obtain tau-PET network for a subject of interest (Fig. 1): To create a reference metabolic network, we utilized scans from a control group comprising healthy individuals. SUVRs of each pair of brain regions were computed with partial Pearson correlation analysis (controlling for age and gender), resulting network matrix labeled as RNet. Next, we added a subject to the control group, forming a new group to construct a perturbed network matrix, labeled as PNet. By calculating the difference between PNet and RNet, we obtained the residual network, which depicted the variation after introducing that subject. Each edge in the residual network indicated the degree of deviation from the normal value observed in the control group. Normally, tau-PET network is with weak nodes and few connected edges. However, when there are alterations in tau deposition, the network strength increases accordingly. This difference network is then converted into a Z-score matrix (ZCC) with Z-test:

$$\text{ZCC} = \frac{\text{PNet} - \text{RNet}}{\frac{1 - \text{RNet}^2}{n-1}} \quad (1)$$

Table 1. Subject characteristics.

	ADNI				
	CN- (n = 48)	CN+ (n = 26)	EMCI (n = 35)	LMCI (n = 32)	AD (n = 40)
Gender (male/female)	21/27	11/15	25/10	20/12	26/14
Age (years)	70.28(±7.12)	73.37(±7.11)	75.77(±6.51)	76.14(±7.5)	75.31(±7.87)
Education (years)	16.67(±2.10)	16.65(±2.02)	17.14(±2.75)	16.75(±2.67)	15.48(±2.68)
MMSE	29.15(±1.06)	28.81(±1.21)	28.34(±1.84)	27.22(±2.27)	23.63(±2.54)
CDR	0.01(±0.07)	0	0.31(±0.24)	0.53(±0.17)	0.74(±0.25)
	HABS				
	CN- (n = 34)	CN+ (n = 21)	MCI (n = 11)		
Gender (male/female)	15/19	9/12	2/9		
Age (years)	77.63(±4.93)	76.96(±5.63)	81.95(±5.17)		
Education (years)	16.29(±2.48)	15.95(±2.73)	16.27(±2.34)		
MMSE	29.62(±0.54)	8.57(±1.33)	26.73(±2.09)		
CDR	0.07(±0.18)	0.1(±0.2)	0.45(±0.14)		

**Fig. 1.** The workflow to construct an individual tau-PET network.

Z-score represents the connection strength between the 2 regions. An individual ZCC matrix comprises 2556 edges connecting 72 brain regions in the Desikan–Killiany atlas (Desikan et al. 2006).

Following that, certain network features were assessed. For the individual network, the sum in Z-score of ZCC matrix was computed as the overall connectivity strength (**S**), which together with SUVR was later regressed against MMSE scores. We binarized the ZCC matrix and established a network threshold of 5% significance, equating to a Z-score of 1.96 and indicating severe irregularity at that edge. The global clustering coefficient (**C**) was then quantified to quantify a network's segregation by reflecting the degree of aggregation between a particular node and nearby nodes. The average clustering coefficient of a network with **m** nodes is the average of the clustering coefficients at all nodes:

$$C = \frac{1}{m} \sum_i C_i = \frac{1}{m} \sum_i \frac{2t_i}{k_i(k_i - 1)} \quad (2)$$

C_i is the clustering coefficient at node **i**, k_i is the number of edges connecting node **i**, and t_i is the actual number of edges between node **i** and adjacent nodes. Global efficiency (**E**) measures

the network integration by measuring the shortest path length between all pairs of nodes:

$$E = \frac{1}{m(m-1)} \sum_{i \neq j} \frac{1}{d_{ij}} \quad (3)$$

d_{ij} is the shortest path length between node **i** and **j**.

Intra- and inter-cluster abnormality examination

Additionally, 7 functional clusters in the brain were identified, i.e. medial temporal lobe (MTL), cognitive control network (CCN), executive control network (ECN), default mode network (DMN), visual network (VIS), somatomotor network (SM), and language network (LAN). Each cluster contains brain regions associated with a certain function, and their definition can be found in Espinoza et al. (2018). Within each cluster, the connectivity strength was examined and compared with the composite SUVR and MTL SUVR in terms of staging capability. Specifically, we are interested in the sensitivity to early disease conversion before MCI. We also computed Cohen's effect size to measure the effectiveness of the staging using each cluster-based biomarker.

Furthermore, each functional cluster was regarded as a mega-node and built 7×7 individual covariance network. The analysis in-between clusters was similar to the one in the preceding section with the main distinction is that a node is a cluster of regions.

Analysis of group heterogeneity

The heterogeneity of the subjects was examined at each disease stage. Pearson correlation coefficient of perturbation networks at the same disease stage was calculated to highlight similarities between all paired Z-scores. We then examined whether this heterogeneity affected the difference at the group level. Group-level networks were built for the ADNI cohort's control and patient group, and their difference was compared against the average individual-level network.

Analysis of patients with disease conversion

We examined subjects with confirmed disease conversion to see how well the topological analysis reflected individual disease progression. One subject has converted from cognitively normal (CN-) to early MCI, while another subject has converted from CN+ to late MCI (demographical information in [Supplementary Table S1](#)). Tau-PET networks before and after the patient's conversion were then built. The change in connectivity strength was compared with the change in SUVR.

Statistical analysis

All statistical analyses were performed using the R language (version 4.2.1, R Foundation for Statistical Computing). Pearson correlation was used to assess the relationship for paired correlation between 2 variables unless stated otherwise. Comparisons of the biomarker among subject groups were made using the Kruskal–Wallis test. Cohen's effect size was used to measure the effectiveness in separating subject groups. A threshold of 0.05 was selected as the level of significance.

Results

Global topological features are associated with disease progression

[Figure 2](#) shows the histograms of global clustering coefficient and efficiency at each subject group. For ADNI, both indices displayed an upward trend from the CN- to the Alzheimer's disease stage. They were statistically different between CN+ and EMCI, EMCI and LMCI, and LMCI and AD (all $P < 0.05$). For HABS, there is a significant difference between CN- and MCI, as well as CN+ and MCI (all $P < 0.01$). However, when comparing the CN- and CN+, neither ADNI nor HABS shows a difference in the clustering coefficient or efficiency. This suggests that the global topological features are sensitive to the staging but not the change in a prodromal stage that typically associated with early amyloid- β deposition.

Individual connectivity strengths are correlated with cognitive assessment

Spearman correlation coefficients between the subject's mean Z-scores, composite SUVR, and corresponding MMSE scores are shown in [Fig. 3](#). For ADNI and HABS, Z-scores were inversely proportional to MMSE with rho value of -0.55 and -0.36 , respectively. SUVR was likewise found to be inversely proportional to MMSE with slightly inferior correlations (rho value -0.51 and -0.28). All correlations were statistically significant ($P < 0.01$).

Topological features are better at staging than SUVR

The tau accumulation patterns were correlated to disease stages. The absolute mean Z-score within 7 functional clusters was shown in [Fig. 4](#) and [Fig. 5](#). Connectivity in certain functional clusters, as biomarkers, can differentiate 4 subject groups ([Fig. 4](#)). For ADNI, the biomarkers that distinguished CN+ from EMCI, EMCI from LMCI, and LMCI from AD ($P < 0.01$) were intra-connectivity strength within MTL, ECN and LAN. The intra-connectivity strength within LAN was most effective in distinguishing the CN+ and EMCI groups. Furthermore, whether topological biomarkers can differentiate CN subgroups (CN- and CN+) was evaluated ([Fig. 5](#)). For ADNI, Z-scores within MTL, DMN, and VIS provide significant differentiation ($P < 0.01$). Overall, the performance of the topological biomarkers outperformed SUVRs. Composite SUVR and MTL SUVR at various stages increase with the disease progression, albeit their capability in early MCI differentiation was restricted.

For the validation cohort HABS, again MTL, ECN, VIS, and DMN contain the most significant biomarkers for distinguishing CN+ and MCI stages. Also similarly, MTL, CCN, and VIS performed better than SUVRs in differentiating CN- and CN+ ($P < 0.01$). Cohen's effect sizes showed consistent results from above comparison for both ADNI and HABS cohorts ([Supplementary Tables S2](#) and [S3](#)). Cluster connectivity Z-scores result in larger effect sizes observed in all comparisons, again indicating topological analysis can differentiate disease stages more effectively than SUVR measures.

[Figure 6](#) depicts the unidirectional connections between the 7 functional clusters, represented by a 7×7 truncated matrix. For ADNI, the connections between functional clusters become increasingly complex as the stage progresses from CN to AD. There is a difference in connection abnormalities between CN- and CN+ stages, although not statistically significant. The connections associated with MTL demonstrated a high degree of connectivity (MTL to VIS connection, Z-scores EMCI:2.16, LMCI:5.49, AD:9.96). For HABS, the connectivity also tends to get more complex as the stage progresses from CN- to MCI. When progressing from CN- to CN+ stage, the connections from VIS to ECN, DMN, SM showed significant anomalies (Z-scores of 2.41, 2.78, and 2.89, respectively). When progressing from CN+ to MCI stage, the connections from VIS, MTL, and CCN to other clusters are significant with most Z-scores greater than 2.16. This demonstrates that MTL and VIS hubs are indication of early Alzheimer's disease which is congruent with the clusters discovered in the previous section.

Connectivity pattern reveals heterogeneity in patients

For ADNI, the mean Pearson correlation coefficients between subjects were 0.97 ± 0.001 (CN-), 0.95 ± 0.01 (CN+), 0.94 ± 0.02 (EMCI), 0.86 ± 0.06 (LMCI), and 0.77 ± 0.07 (AD). Similarly, for HABS, the mean Pearson correlation coefficients were 0.97 ± 0.001 (CN-), 0.92 ± 0.03 (CN+), and 0.82 ± 0.05 (MCI). This indicates that heterogeneity among patient groups increase as the disease progress.

For ADNI, correlation coefficients between the average individual-level difference network and group-level difference network were 0.53 (CN+), 0.49 (EMCI), 0.52 (LMCI), and 0.42 (AD), all $P < 0.01$. However, when looking at each individual network, they have low average correlation with the group-level difference network, which were 0.16 ± 0.08 (CN+), 0.18 ± 0.06 (EMCI), 0.17 ± 0.13 (LMCI), and 0.20 ± 0.08 (AD). Similar findings were found for HABS, implying that each subject contributed to group-level difference differently.

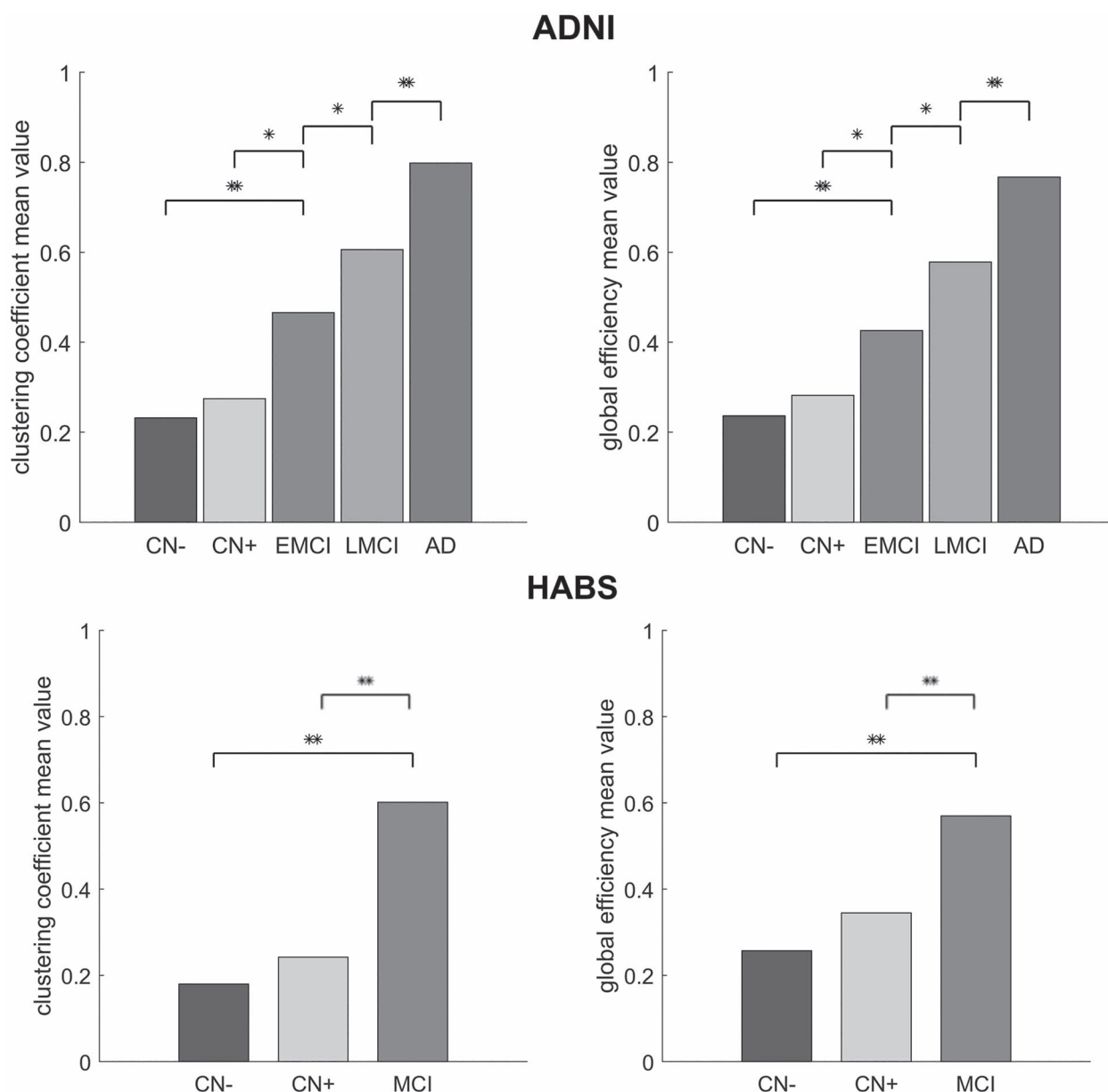


Fig. 2. Histogram of the global clustering coefficient and efficiency calculated from the scans at different stages (* $P < 0.05$, ** $P < 0.01$).

Converted subjects have more connectivity changes than SUVR

Figure 7 shows the change of abnormal connectivity and SUVR in the CCN for 2 subjects whose disease status converted in 36 months. Figure 7A shows a subject converted from CN- to EMCI stage. After conversion, the composite SUVR decreased (-2.9%), while the number of abnormal edges increased (48.9%). Figure 7B shows a subject converted from CN+ to LMCI, with the change in connectivity (102.5%) being more noticeable than the change in SUVR (12.8%). This suggests the change in connectivity strength from the baseline may be more sensitive to an individual's subtle or atypical tau accumulation.

Discussion and conclusion

Tau is the strongest driver of cognitive decline in Alzheimer's disease, which can be used to indicate disease progression

(Busche and Hyman 2020; D'Errico and Meyer-Luehmann 2020). Individual spatial variability in tau deposition limits SUVR-based quantification using PET imaging. Topological analysis of tau deposition pattern may better represent Alzheimer's disease progression. We intend to study tau PET image from topological perspective across Alzheimer's disease stages at both individual and group levels. Tau accumulation was measured cross-sectionally and compared using proposed topological and conventional regional methods. The derived network is not a true functional connectivity network but a perturbation to the population's normal deposition level. Our goal was not to "diagnose" Alzheimer's disease but to test suitable biomarkers for staging, early detection, and to associate with progression. Overall, cluster-based topological data analysis outperformed composite SUVR and medial temporal lobe SUVR. This is more obvious when using the significant topological biomarkers to identify the prodromal sign of Alzheimer's disease. We also found that compared with subjects having confirmed or developing

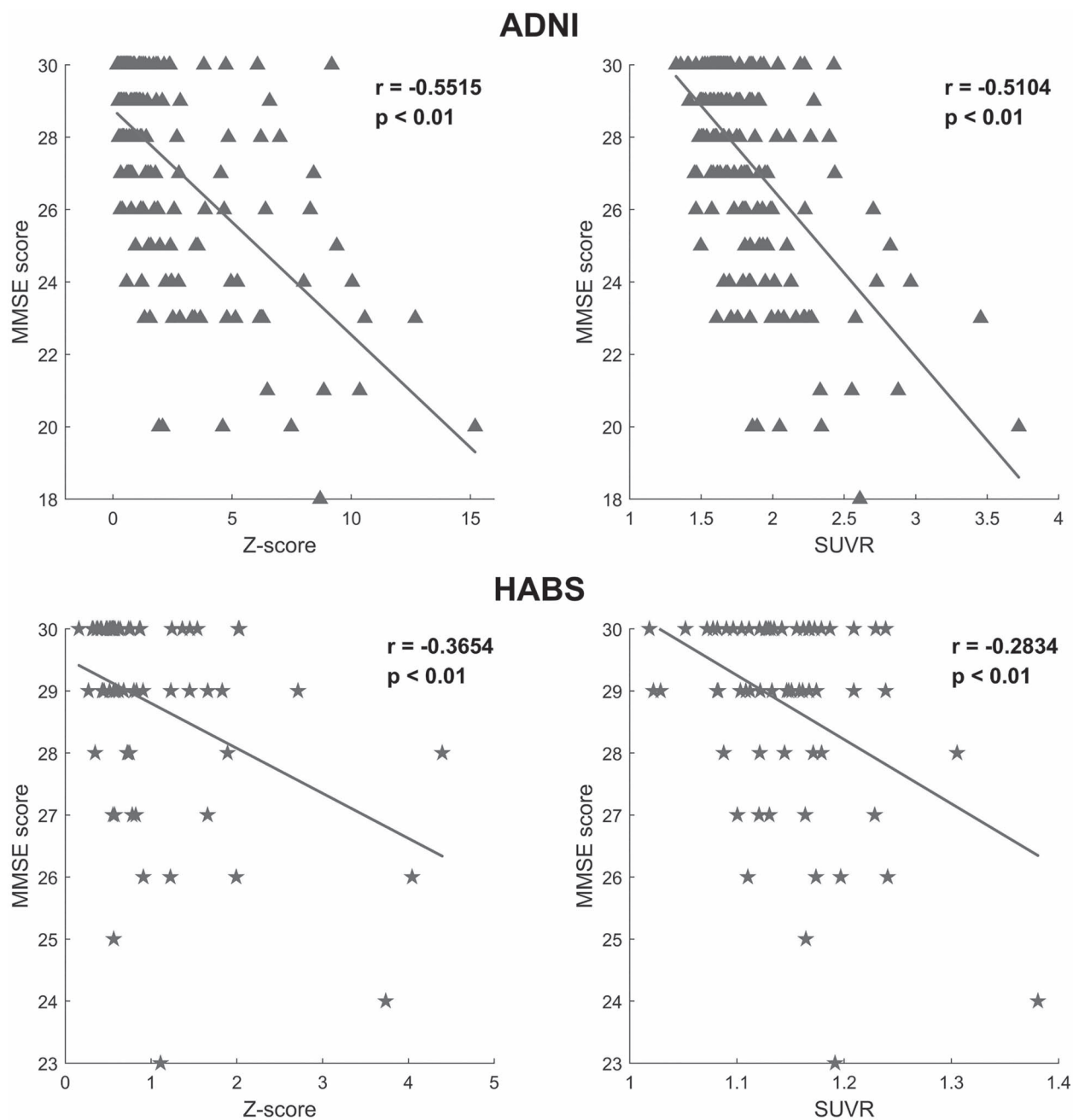


Fig. 3. Spearman correlations between measures (network Z-scores/SUVR) and cognitive assessment scores (MMSE).

disease status, topological features of the normal-aged subjects did not change much. This suggests staging of a subject at prodromal stage is less likely to be misinterpreted as normal aged condition. Using ^{18}F -florotau PET scans, these findings were validated in ADNI and replicated in an independent cohort HABS.

From a topological perspective, there is significant heterogeneity among patients even within the same disease group in both data cohorts. This observation is consistent with previous studies (Lambon Ralph et al. 2003; Murray et al. 2011; Whitwell et al. 2012; Petersen et al. 2019; Young et al. 2022), which showed tau pathophysiology has a focal aggregation and highly heterogeneous pattern of progression through the brain. We believe the proposed biomarkers will be sensitive to the change in tau deposition after early treatment, which could be highly heterogeneous and

subtle. This can be indirectly proven in Fig. 7, where the change in connectivity was more pronounced in some converted cases than in visual or SUVR assessment. Moreover, it is of great value to see whether the extracted topological pattern can predict the individual treatment effect.

Our results are consistent in ADNI and HABS cohorts, suggesting the modeling approach applies to a diverse population. However, the overall staging results in ADNI were less accurate than in HABS. The sampled demographic differences may explain this phenomenon. Most ADNI patients were amnesic and over the age of 70, while HABS patients had a more diverse range of Alzheimer's disease phenotypes that most started at a young age. Another issue is, HABS did not differentiate early and late MCI and did not contain any AD subjects. Additionally, differences in scanner model and imaging protocols might affect our results.

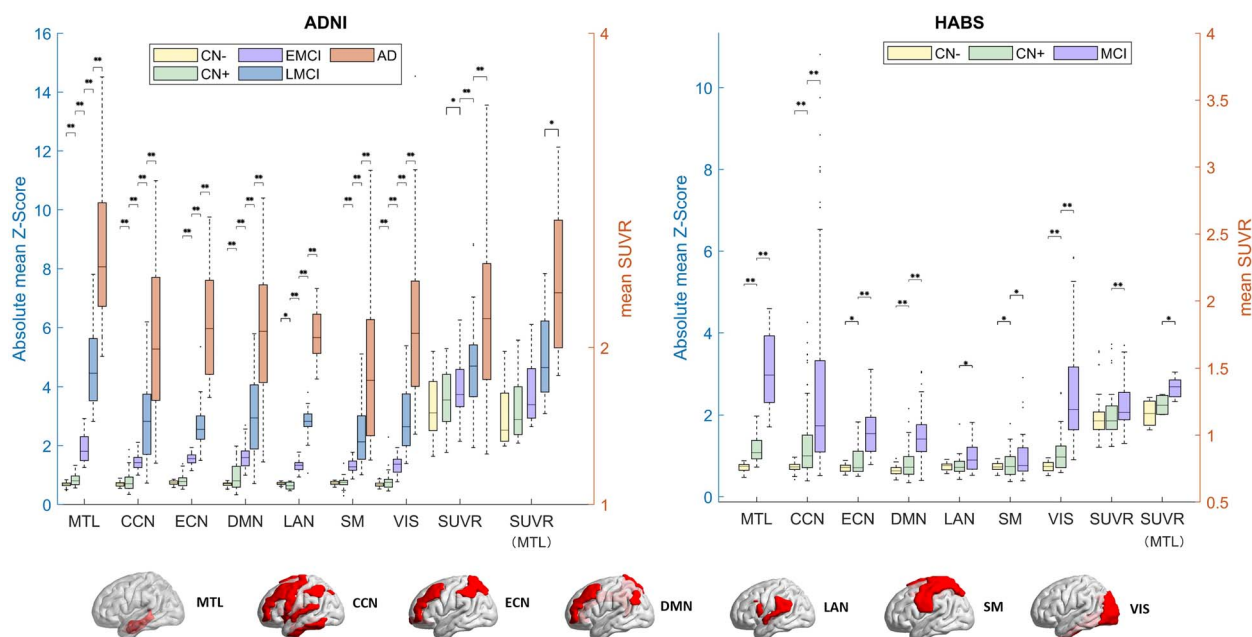


Fig. 4. Distributions of the average abnormal connectivity within each functional cluster and SUVRs for subject group at disease stages (* $P < 0.05$, ** $P < 0.01$).

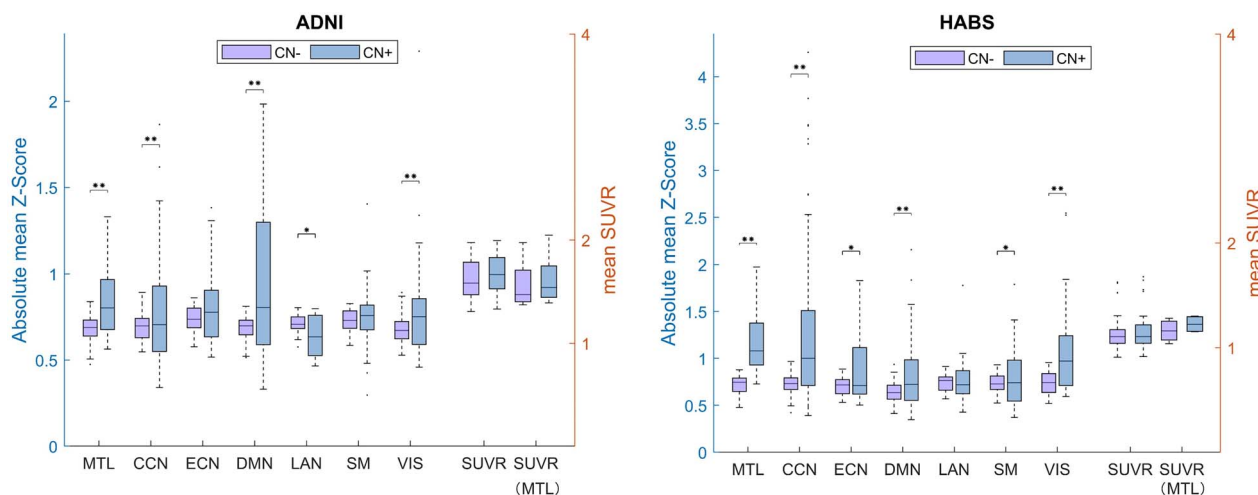


Fig. 5. Distributions of the average abnormal connectivity within each cluster and SUVRs for CN- and CN+ group (** $P < 0.01$).

Normalizing the PET images from different cohorts would allow to build up a standardized analysis model.

The inclusion of partial volume correction could recover the uptake especially for hippocampus that is known prone to partial volume effect (Groot et al. 2022). As a result, discriminative accuracy between impaired and unimpaired individuals was shown to improve in cross-sectional study (Schwarz et al. 2021). This can be very important for early detection as the deposition can be subtle and limited to small areas. The network connectivity in this study also benefits from these corrections as the network was built up from SUVR values at parcellated regions.

The small cohort size is a limitation of this study. FDA approved ^{18}F -Flortaucipir PET in 2020, so the number of available scans may be insufficient for robust statistical analyses especially for the longitudinal study. Currently only 2 converted cases with follow-up scans were investigated, but more are required to validate

the potential of the proposed framework in predicting the future disease status. Additional data from other data cohorts would help validate the current framework (Bucci et al. 2021; Leuzy et al. 2022), especially for individuals with atypical Alzheimer's disease symptoms before age of 65. The second limitation is that tau tangles are not Alzheimer's disease specific. ^{18}F -flortaucipir both binds to non-Alzheimer's disease tau isoforms and non-tau processes (Xia et al. 2013; Schonhaut et al. 2017; Smith et al. 2017; Leuzy et al. 2019). It also has considerable unspecific off-target binding in the basal ganglia, hippocampus, and choroid plexus (Barthel 2020), which may confound the accurate SUVR quantification. Although we believe such an impact is less sensitive for a topological analysis as suggested by the staging performance in Figs 4 and 5, still, our findings need further replication with second-generation tau-PET tracers with a higher specific binding (Lohith et al. 2019; Mueller et al. 2020; Tagai et al. 2021).

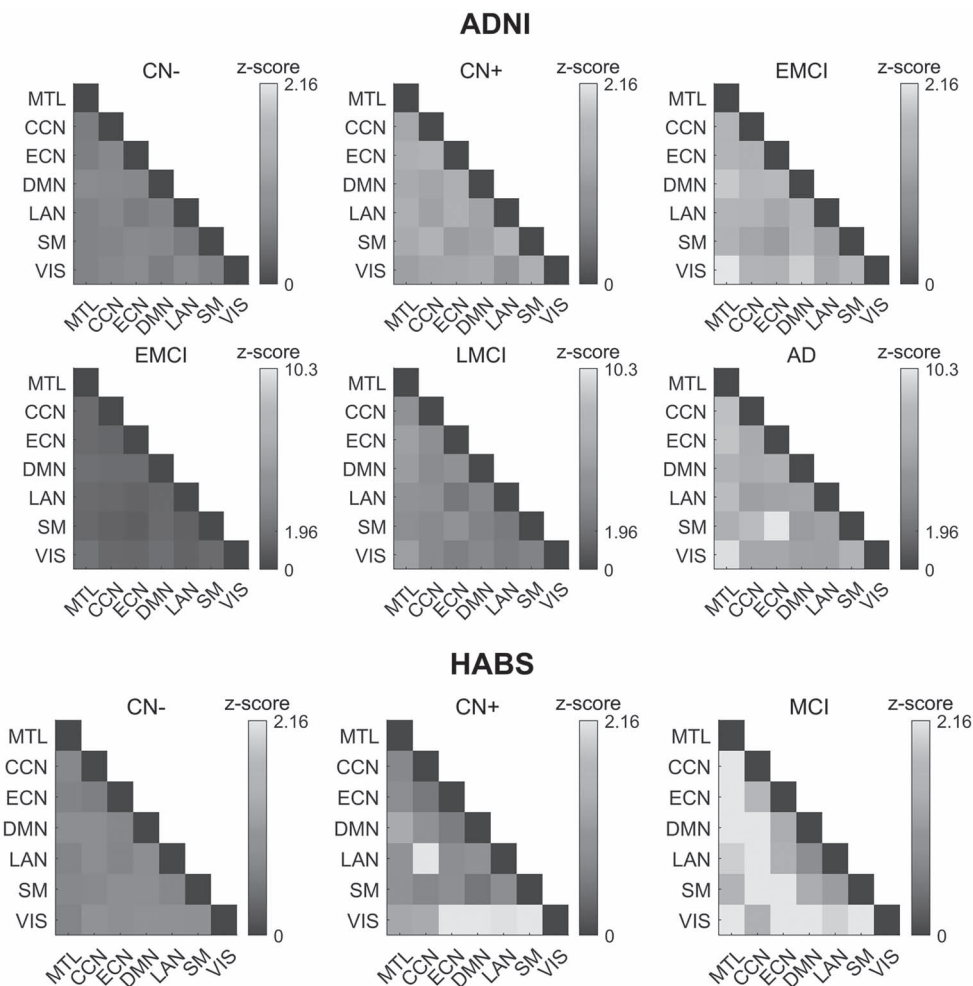


Fig. 6. Abnormal connectivity between functional clusters at different disease stages. The difference in connectivity matrices was assessed between adjacent stages. In ADNI, all pairwise matrices were significantly different ($P < 0.05$) except the one between CN+ and EMCI ($P = 0.06$). In HABS, differences between stages are all significant ($P < 0.01$).

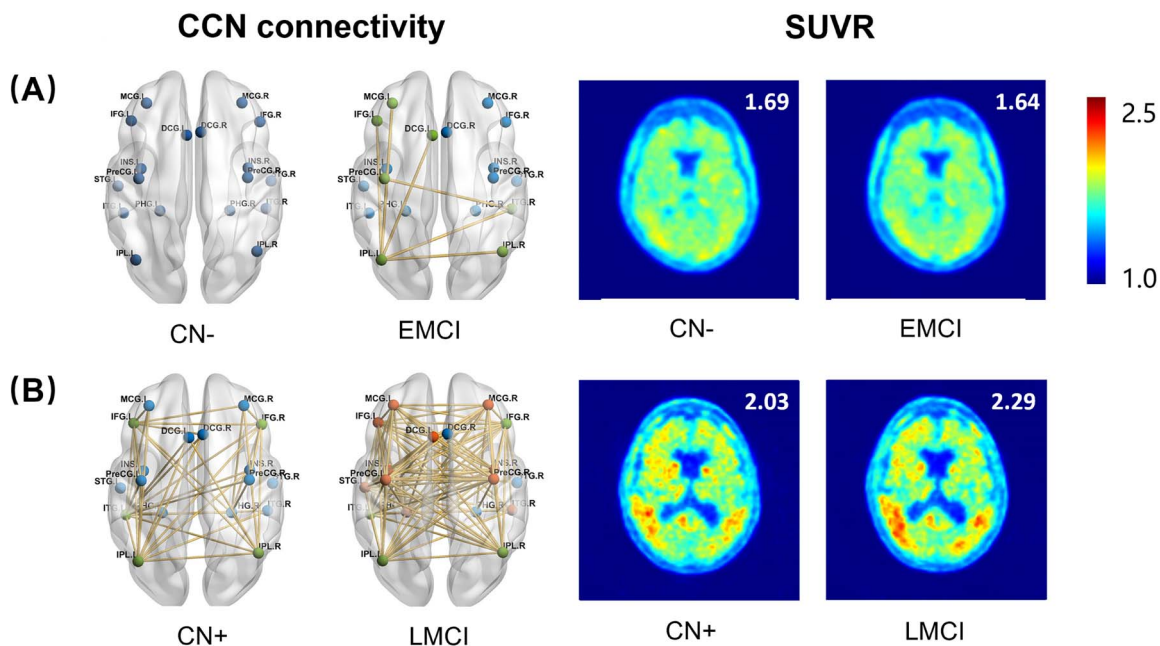


Fig. 7. For subjects (A) and (B), the change of CCN connectivity and SUVR before and after disease conversion. The red nodes indicate abnormal brain regions that appear after conversion, the green nodes indicate abnormal both before and after conversion, and the blue nodes indicate regions with insignificant abnormal connections at all times. The yellow lines are the significant connections between connected nodes.

Supplementary material

Supplementary material is available at *Cerebral Cortex* online.

Fundings

This work is supported by the Scientific Instrument Innovation Team of the Chinese Academy of Sciences (GJJSTD20180002), the Key Laboratory for Magnetic Resonance and Multimodality Imaging of Guangdong Province (2020B1212060051), Shenzhen Science and Technology Innovation Committee (20220531100209020), and Department of Science and Technology of Guangdong Province (2022A1515110716).

Conflict of interest statement: The authors of this manuscript declare relationships with the following companies: Yun Zhou is an employee of United Imaging Healthcare.

Author contributions

Jie Ding (Conceptualization, Formal analysis, Writing—original draft, Writing—review & editing), Chushu Shen (Data curation, Methodology, Software, Writing—review & editing), Zhenguo Wang (Data curation, Software, Validation, Visualization, Writing—review & editing), Yongfeng Yang (Project administration, Resources, Validation, Writing—review & editing), Georges El Fakhri (Methodology, Writing—review & editing), Jie Lu (Investigation, Writing—review & editing), Dong Liang (Funding acquisition, Project administration, Resources), Hairong Zheng (Resources, Supervision), Yun Zhou (Methodology, Writing—review & editing), Tao Sun (Conceptualization, Data curation, Funding acquisition, Investigation, Methodology, Project administration, Resources, Software, Supervision, Validation, Visualization, Writing—original draft, Writing—review & editing).

Data availability

Data used in preparation of this article were obtained from the ADNI database (adni.loni.usc.edu). As such, the investigators within the ADNI contributed to the design and implementation of ADNI and/or provided data but did not participate in analysis or writing of this report. A complete listing of ADNI investigators can be found at http://adni.loni.usc.edu/wp-content/uploads/how_to_apply/ADNI_Acknowledgement_List.pdf. Data used in preparation of this article were also obtained from the Harvard Aging Brain Study (HABS; <https://habs.mgh.harvard.edu/>). The HABS was launched in 2010, funded by the National Institute on Aging, and is led by principal investigators Reisa A. Sperling, MD, and Keith Johnson, MD, at Massachusetts General Hospital/Harvard Medical School.

References

Barthel H. First tau PET tracer approved: toward accurate in vivo diagnosis of Alzheimer disease. *J Nucl Med*. 2020;61:1409–1410.

Biel D, Brendel M, Rubinski A, Buerger K, Janowitz D, Dichgans M, Franzmeier N, (ADNI) for the ADNI. Tau-PET and in vivo Braak-staging as prognostic markers of future cognitive decline in cognitively normal to demented individuals. *Alzheimers Res Ther*. 2021;13:137.

Braak H, Braak E. Staging of alzheimer's disease-related neurofibrillary changes. *Neurobiol Aging*. 1995;16:271–278.

Bucci M, Chiotis K, Nordberg A. Alzheimer's disease profiled by fluid and imaging markers: tau PET best predicts cognitive decline. *Mol Psychiatry*. 2021;26:5888–5898.

Busche MA, Hyman BT. Synergy between amyloid- β and tau in Alzheimer's disease. *Nat Neurosci*. 2020;23:1183–1193.

Chien DT, Bahri S, Szardenings AK, Walsh JC, Mu F, Su M-Y, Shankle WR, Elizarov A, Kolb HC. Early clinical PET imaging results with the novel PHF-tau Radioligand [F-18]-T807. *J Alzheimers Dis*. 2013;34:457–468.

Cho H, Choi JY, Hwang MS, Lee JH, Kim YJ, Lee HM, Lyoo CH, Ryu YH, Lee MS. Tau PET in Alzheimer disease and mild cognitive impairment. *Neurology*. 2016;87:375 LP – 383.

Chung J, Yoo K, Kim E, Na DL, Jeong Y. Glucose metabolic brain networks in early-onset vs. late-onset Alzheimer's disease. *Front Aging Neurosci*. 2016;8:1–11.

D'Errico P, Meyer-Luehmann M. Mechanisms of pathogenic tau and A β protein spreading in Alzheimer's disease. *Front Aging Neurosci*. 2020;12:1–10.

Dagley A, LaPoint M, Huijbers W, Hedden T, McLaren DG, Chatwal JP, Papp KV, Amariglio RE, Blacker D, Rentz DM, et al. Harvard aging brain study: dataset and accessibility. *NeuroImage*. 2017;144:255–258.

de Schotten MT, Forkel SJ. The emergent properties of the connected brain. *Science*. 2022;378(80):505–510.

Desikan RS, Ségonne F, Fischl B, Quinn BT, Dickerson BC, Blacker D, Buckner RL, Dale AM, Maguire RP, Hyman BT, et al. An automated labeling system for subdividing the human cerebral cortex on MRI scans into gyral based regions of interest. *NeuroImage*. 2006;31:968–980.

Edmonds EC, McDonald CR, Marshall A, Thomas KR, Eppig J, Weigand AJ, Delano-Wood L, Galasko DR, Salmon DP, Bondi MW, et al. Early versus late MCI: improved MCI staging using a neuropsychological approach. *Alzheimers Dement*. 2019;15:699–708.

Espinoza FA, Vergara VM, Reyes D, Anderson NE, Harenski CL, Decety J, Rachakonda S, Damaraju E, Rashid B, Miller RL, et al. Aberrant functional network connectivity in psychopathy from a large (N = 985) forensic sample. *Hum Brain Mapp*. 2018;39:2624–2634.

Ferreira D, Nordberg A, Westman E. Biological subtypes of Alzheimer disease. *Neurology*. 2020;94:436 LP – 448.

Galvin JE, Price JL, Yan Z, Morris JC, Sheline YI. Resting bold fMRI differentiates dementia with Lewy bodies vs Alzheimer disease. *Neurology*. 2011;76:1797 LP–1803.

Groot C, Villeneuve S, Smith R, Hansson O, Ossenkoppele R. Tau PET imaging in neurodegenerative disorders. *J Nucl Med*. 2022;63:20S–26S.

Huang SY, Hsu JL, Lin KJ, Liu HL, Wey SP, Hsiao IT. Characteristic patterns of inter- and intra-hemispheric metabolic connectivity in patients with stable and progressive mild cognitive impairment and Alzheimer's disease. *Sci Rep*. 2018;8:1–11.

Huang SY, Hsu JL, Lin KJ, Hsiao IT. A novel individual metabolic brain network for 18-FDG PET imaging. *Front Neurosci*. 2020;14:1–15.

Iturria-Medina Y, Canales-Rodríguez EJ, Melie-García L, Valdés-Hernández PA, Martínez-Montes E, Alemán-Gómez Y, Sánchez-Bornot JM. Characterizing brain anatomical connections using diffusion weighted MRI and graph theory. *NeuroImage*. 2007;36:645–660.

Jack CR, Wiste HJ, Weigand SD, Therneau TM, Lowe VJ, Knopman DS, Gunter JL, Senjem ML, Jones DT, Kantarci K, et al. Defining imaging biomarker cut points for brain aging and Alzheimer's disease. *Alzheimers Dement*. 2017;13:205–216.

- Johnson KA, Schultz A, Betensky RA, Becker JA, Sepulcre J, Rentz D, Mormino E, Chhatwal J, Amariglio R, Papp K, et al. Tau positron emission tomographic imaging in aging and early Alzheimer disease. *Ann Neurol*. 2016;79:110–119.
- Lambon Ralph MA, Patterson K, Graham N, Dawson K, Hodges JR. Homogeneity and heterogeneity in mild cognitive impairment and Alzheimer's disease: a cross-sectional and longitudinal study of 55 cases. *Brain*. 2003;126:2350–2362.
- Landau SM, Mintun MA, Joshi AD, Koeppe RA, Petersen RC, Aisen PS, Weiner MW, Jagust WJ, Initiative for the ADN. Amyloid deposition, hypometabolism, and longitudinal cognitive decline. *Ann Neurol*. 2012;72:578–586.
- Leuzy A, Chiotis K, Lemoine L, Gillberg P-G, Almkvist O, Rodriguez-Veitez E, Nordberg A. Tau PET imaging in neurodegenerative tauopathies—still a challenge. *Mol Psychiatry*. 2019;24:1112–1134.
- Leuzy A, Smith R, Cullen NC, Strandberg O, Vogel JW, Binette AP, Borroni E, Janelidze S, Ohlsson T, Jögi J, et al. Biomarker-based prediction of longitudinal tau positron emission tomography in Alzheimer disease. *JAMA Neurol*. 2022;79:149–158.
- Li K, Chen GH. Statistical properties of cerebral CT perfusion imaging systems. Part II. Deconvolution-based systems. *Med Phys*. 2019;46:4881–4897.
- Lohth TG, Bennacef I, Vandenberghe R, Vandenbulcke M, Salinas CA, Declercq R, Reynders T, Florestina Telan-Choing N, Riffel K, Celen S, et al. Brain imaging of Alzheimer dementia patients and elderly controls with 18 F-MK-6240, a PET tracer targeting neurofibrillary tangles. *J Nucl Med*. 2019;60:107–114.
- Maass A, Landau S, Baker SL, Horng A, Lockhart SN, La Joie R, Rabinovici GD, Jagust WJ. Comparison of multiple tau-PET measures as biomarkers in aging and Alzheimer's disease. *NeuroImage*. 2017;157:448–463.
- Montal V, Diez I, Kim CM, Orwig W, Buechekú E, Gutiérrez-Zúñiga R, Bejanin A, Pegueroles J, Dols-Icardo O, Vannini P, et al. Network tau spreading is vulnerable to the expression gradients of APOE and glutamatergic-related genes. *Sci Transl Med*. 2022;14:eabn7273.
- Mueller A, Bullich S, Barret O, Madonia J, Berndt M, Papin C, Perrotin A, Koglin N, Kroth H, Pfeifer A, et al. Tau PET imaging with 18F-PI-2620 in patients with Alzheimer disease and healthy controls: a first-in-humans study. *J Nucl Med*. 2020;61:911–919.
- Murray ME, Graff-Radford NR, Ross OA, Petersen RC, Duara R, Dickson DW. Neuropathologically defined subtypes of Alzheimer's disease with distinct clinical characteristics: a retrospective study. *Lancet Neurol*. 2011;10:785–796.
- Ossenkoppele R, Schonhaut DR, Schöll M, Lockhart SN, Ayakta N, Baker SL, O'Neil JP, Janabi M, Lazaris A, Cantwell A, et al. Tau PET patterns mirror clinical and neuroanatomical variability in Alzheimer's disease. *Brain*. 2016;139:1551–1567.
- Ossenkoppele R, Iaccarino L, Schonhaut DR, Brown JA, La Joie R, O'Neil JP, Janabi M, Baker SL, Kramer JH, Gorno-Tempini ML, et al. Tau covariance patterns in Alzheimer's disease patients match intrinsic connectivity networks in the healthy brain. *NeuroImage Clin*. 2019;23:1–13.
- Pelkmans W, Ossenkoppele R, Dicks E, Strandberg O, Barkhof F, Tijms BM, Pereira JB, Hansson O. Tau-related grey matter network breakdown across the Alzheimer's disease continuum. *Alzheimers Res Ther*. 2021;13:1–11.
- Petersen RC, Aisen PS, Beckett LA, Donohue MC, Gamst AC, Harvey DJ, Jack CR, Jagust WJ, Shaw LM, Toga AW, et al. Alzheimer's Disease Neuroimaging Initiative (ADNI). *Neurology*. 2010;74:201 LP–209.
- Petersen C, Nolan AL, de Paula França Resende E, Miller Z, Ehrenberg AJ, Gorno-Tempini ML, Rosen HJ, Kramer JH, Spina S, Rabinovici GD, et al. Alzheimer's disease clinical variants show distinct regional patterns of neurofibrillary tangle accumulation. *Acta Neuropathol*. 2019;138:597–612.
- Rousset OG, Ma Y, Evans AC. Correction for partial volume effects in PET: principle and validation. *J Nucl Med*. 1998;39:904–911.
- Rubinov M, Sporns O. Complex network measures of brain connectivity: uses and interpretations. *NeuroImage*. 2010;52:1059–1069.
- Sala A, Perani D. Brain molecular connectivity in neurodegenerative diseases: recent advances and new perspectives using positron emission tomography. *Front Neurosci*. 2019;13:1–15.
- Sala A, Lizarraga A, Caminiti SP, Calhoun VD, Eickhoff SB, Habeck C, Jamadar SD, Perani D, Pereira JB, Veronese M, et al. Brain connectomics: time for a molecular imaging perspective? *Trends Cogn Sci*. 2023;27:P353–P366.
- Schöll M, Lockhart SN, Schonhaut DR, O'Neil JP, Janabi M, Ossenkoppele R, Baker SL, Vogel JW, Faria J, Schwimmer HD, et al. PET imaging of tau deposition in the aging human brain. *Neuron*. 2016;89:971–982.
- Schonhaut DR, McMillan CT, Spina S, Dickerson BC, Siderowf A, Devous MD Sr, Tsai R, Winer J, Russell DS, Litvan I, et al. 18F-flortaucipir tau positron emission tomography distinguishes established progressive supranuclear palsy from controls and Parkinson disease: a multicenter study. *Ann Neurol*. 2017;82:622–634.
- Schwarz AJ, Yu P, Miller BB, Shcherbinin S, Dickson J, Navitsky M, Joshi AD, Devous MD, Mintun MS. Regional profiles of the candidate tau PET ligand 18F-AV-1451 recapitulate key features of Braak histopathological stages. *Brain*. 2016;139:1539–1550.
- Schwarz CG, Therneau TM, Weigand SD, Gunter JL, Lowe VJ, Przybelski SA, Senjem ML, Botha H, Vemuri P, Kantarci K, et al. Selecting software pipelines for change in flortaucipir SUVR: balancing repeatability and group separation. *NeuroImage*. 2021;238:118259.
- Seghier ML, Price CJ. Interpreting and utilising Intersubject variability in brain function. *Trends Cogn Sci*. 2018;22:517–530.
- Smith R, Schöll M, Widner H, van Westen D, Svenningsson P, Hägerström D, Ohlsson T, Jögi J, Nilsson C, Hansson O. In vivo retention of 18F-AV-1451 in corticobasal syndrome. *Neurology*. 2017;89:845–853.
- Sun T, Wang Z, Wu Y, Gu F, Li X, Bai Y, Shen C, Hu Z, Liang D, Liu X, et al. Identifying the individual metabolic abnormalities from a systemic perspective using whole-body PET imaging. *Eur J Nucl Med Mol Imaging*. 2022;49:2994–3004.
- Tagai K, Ono M, Kubota M, Kitamura S, Takahata K, Seki C, Takado Y, Shinotoh H, Sano Y, Yamamoto Y, et al. High-contrast in vivo imaging of tau pathologies in Alzheimer's and non-Alzheimer's disease Tauopathies. *Neuron*. 2021;109:42–58.e8.
- Tian M, Civelek AC, Carrio I, Watanabe Y, Kang KW, Murakami K, Garibotto V, Prior JO, Barthel H, Zhou R, et al. International consensus on the use of tau PET imaging agent 18F-flortaucipir in Alzheimer's disease. *Eur J Nucl Med Mol Imaging*. 2022;49:895–904.
- Wang M, Jiang J, Yan Z, Alberts I, Ge J, Zhang H, Zuo C, Yu J, Rominger A, Shi K. Individual brain metabolic connectome indicator based on Kullback-Leibler divergence similarity estimation predicts progression from mild cognitive impairment to Alzheimer's dementia. *Eur J Nucl Med Mol Imaging*. 2020;47:2753–2764.
- Whitwell JL, Dickson DW, Murray ME, Weigand SD, Tosakulwong N, Senjem ML, Knopman DS, Boeve BF, Parisi JE, Petersen RC, et al.

- Neuroimaging correlates of pathologically defined subtypes of Alzheimer's disease: a case-control study. *Lancet Neurol.* 2012;11:868–877.
- Whitwell JL, Graff-Radford J, Tosakulwong N, Weigand SD, Machulda MM, Senjem ML, Spychalla AJ, Vemuri P, Jones DT, Drubach DA, et al. Imaging correlations of tau, amyloid, metabolism, and atrophy in typical and atypical Alzheimer's disease. *Alzheimers Dement.* 2018;14:1005–1014.
- Xia C-F, Arteaga J, Chen G, Gangadharmath U, Gomez LF, Kasi D, Lam C, Liang Q, Liu C, Mocharla VP, et al. [18F]T807, a novel tau positron emission tomography imaging agent for Alzheimer's disease. *Alzheimers Dement.* 2013;9:666–676.
- Xia C, Makaretz SJ, Caso C, McGinnis S, Gomperts SN, Sepulcre J, Gomez-Isla T, Hyman BT, Schultz A, Vasdev N, et al. Association of in vivo [18F]AV-1451 tau PET imaging results with cortical atrophy and symptoms in typical and atypical Alzheimer disease. *JAMA Neurol.* 2017;74:427–436.
- Yakushev I, Drzezga A, Habeck C. Metabolic connectivity: methods and applications. *Curr Opin Neurol.* 2017;30:677–685.
- Yakushev I, Ripp I, Wang M, Savio A, Schutte M, Lizarraga A, Bogdanovic B, Diehl-Schmid J, Hedderich DM, Grimmer T, et al. Mapping covariance in brain FDG uptake to structural connectivity. *Eur J Nucl Med Mol Imaging.* 2022;49:1288–1297.
- Young CB, Winer JR, Younes K, Cody KA, Betthauser TJ, Johnson SC, Schultz A, Sperling RA, Greicius MD, Cobos I, et al. Divergent cortical tau positron emission tomography patterns among patients with preclinical Alzheimer disease. *JAMA Neurol.* 2022;79:592–603.
- Zalesky A, Fornito A. A DTI-derived measure of Cortico-cortical connectivity. *IEEE Transactions on Medical Imaging.* 2009;28:1023–1036.